Energy Conversion and Management 321 (2024) 119038

Contents lists available at ScienceDirect

Energy Conversion and Management

journal homepage: www.elsevier.com/locate/enconman

Research Paper

Techno-economic analysis of the direct solar conversion of carbon dioxide into renewable fuels

Abdul Ahad Mamun, Muhammad Anisuzzaman Talukder *

Department of Electrical and Electronic Engineering, Bangladesh University of Engineering and Technology, Dhaka 1205, Bangladesh

ARTICLE INFO

Keywords:
Carbon dioxide reduction
Chemical energy
Renewable Fuels
Direct solar conversion

ABSTRACT

Direct conversion of carbon dioxide (CO_2) using sunlight into commercially viable renewable fuels will be one key solution for decarbonization and storing renewable solar energy. However, the direct conversion of CO_2 using sunlight faces uphill challenges, especially the techno-economic viability (TEV), as the produced fuels must compete with fossil fuels or at least with fossil fuel alternatives, which are cheap. This work proposes an innovative structure design for photoelectrochemical reduction of CO_2 into renewable fuels and performs a detailed techno-economic analysis (TEA) using a generalized gross margin (GM) model. The proposed structure uses low-cost and earth-abundant crystalline silicon-based photoanode with triangle nano-strips on a thin-film substrate to efficiently convert solar energy into renewable fuels. The proposed structure shows 20.01% of power-conversion efficiency (η_{PEC}). The techno-economic GM model considers all relevant cost parameters to assess the TEV of the produced hydrogen (H_2) and hydrocarbon (C_1–C_3) fuels from CO_2 reduction processes. The TEV of the produced renewable fuels is analyzed and presented against critical device parameters, such as the photocurrent density (J), catalyst's durability (t_{dur}), Faradaic efficiency (FE), and catalyst cost (C_{cat}). We also analyzed how sensitively the TEV of the produced fuels depends on the uncertainty of different cost parameters assuming base-, worst-, and optimistic-case scenarios. We find that carbon monoxide (CO) and formic acid (HCOOH) fuels will be commercially viable in the base case, while H_2 and propanol (C_3H_7OH) will be only in the optimistic case.

1. Introduction

Decarbonization of the global environment and reducing fossil fuel dependence are among the prime needs that the world faces at the moment [1,2]. The adverse effects of increased carbon dioxide (CO_2) in the environment are challenging the sustainability of biological lives and impacting the economy dearly [3–6]. For example, in 2023, 40.9 billion metric tons of CO_2 was emitted to the atmosphere from anthropogenic sources, which corresponds to an increase in global mean temperature by ~0.15 °C [7,8]. The economic impact of the temperature rise is a social cost burden as high as $1.70–2.30 trillion between 2020 and 2050 when the aggregate harm to global agricultural productivity, human health, property damage, and energy systems is considered [9–11]. Decarbonization requires a two-pronged approach: Reducing the accumulated CO_2 level and recycling the day-to-day industrial emitted CO_2 [12,13]. Nature has its way of getting rid of naturally emitted CO_2 mainly by converting it into glucose and oxygen (O_2) through photosynthesis—the biological metabolism. [14,15]. However, unlike biological metabolism, the global industrial metabolism lacks CO_2 reduction (CO_2R), leading to an alarming increase in the CO_2 level and disrupting the earth's natural carbon cycle [16,17]. It is crucial to reduce CO_2 emissions rapidly to achieve net-zero and the Paris Agreement goals, keeping global warming below the moderately safe level of 1.5 °C by the year 2050 [18,19].

Several techniques, such as photoelectrochemical, biochemical, thermochemical, and electrochemical cells, use water (H_2O) for CO_2R [20,21]. In addition, combining various techniques, such as photon-enhanced thermionic emission and solid oxide electrolysis cells, with photovoltaics is a promising approach for high-temperature CO_2R [22]. Photoelectrochemical cells (PECs) comprise the photon-harvesting and electrocatalysis processes simultaneously for the direct solar conversion of CO_2 into renewable fuels. PECs have attracted much attention due to their higher efficiency in photo-conversion, tremendous possibility for large-scale industrialization, and not requiring an external power supply during CO_2R reactions (CO_2RR) [23–25]. Semiconductor materials in photoelectrodes contribute to photon harvesting with a high photocurrent density (J), resulting in a faster CO_2RR rate [26,27]. Photoelectrode materials, such as titanium dioxide (TiO_2), tungsten trioxide (WO_3), bismuth vanadate ($BiVO_4$), gallium arsenide (GaAs), and

* Corresponding author.
E-mail address: anis@eee.buet.ac.bd (M.A. Talukder).

https://doi.org/10.1016/j.enconman.2024.119038
Received 7 June 2024; Received in revised form 3 September 2024; Accepted 8 September 2024
Available online 21 September 2024

Nomenclature

Acronyms

2D-G	Two-dimensional conductive graphene
BLS	Bureau of Labor Statistics
c-Si	Crystalline silicon
CO_2R	Carbon dioxide reduction
CO_2RR	Carbon dioxide reduction reaction
DFAFC	Direct formic acid fuel cell
DME	Dimethyl ether
FDTD	Finite-difference time-domain
FEM	Finite Element Method
GDL	Gas diffusion layer
GM	Gross margin
LFC	Levelized fuel cost
MEA	Monoethanolamine
PEC	Photoelectrochemical cell
PEM	Polymer electrolyte membrane
PETE	Photon-enhanced thermionic emission
PML	Perfectly matched layer
PTFE	Polytetrafluoroethylene
PV	Photovoltaic
S-DAC	Solid direct air capture
SOA	State-of-the-art
SOEC	Solid oxide electrolysis cell
SRH	Shockley-Read-Hall
TEA	Techno-economic analysis
TEV	Techno-economic viability

Chemical Formulas

C_2H_4	Ethylene
C_2H_5OH	Ethanol
C_3H_7OH	Propanol
CH_3OH	Methanol
CH_4	Methane
CO	Carbon monoxide
CO_2	Carbon dioxide
$CO+H_2$	Syngas
H_2	Hydrogen gas
H_2O	Water
HCOOH	Formic acid
KOH	Potassium hydroxide
O_2	Oxygen gas

Greek Symbols

η_{PCE}	Power-conversion efficiency (%)
λ	Wavelength (nm)
λ_{BOP}	Balance of plant cost (%)
λ_{cap}	Capital cost ($/stack)
λ_{cat}	Catalyst cost ($/stack)
λ_{COGS}	Cost of goods sold ($)
λ_{cp}	Carbon dioxide capture cost ($/stack)
λ_{elec}	Electrolyte cost ($/stack)
λ_{lab}	Labor cost ($/stack)
λ_{op}	Operation cost ($/stack)
λ_{ph}	Photoanode cost ($/stack)
λ_R	Revenue ($)
λ_{sc}	Stack casing cost ($/stack)
λ_{sep}	Fuel separation cost ($/stack)

Symbols

A_λ	Absorption spectrum (%)
c	Speed of light (ms^{-1})
C_{cat}	Catalyst cost ($/mg)
E_0	Standard reduction potential (V)
E_{red}	Reduction potential (V)
F	Faraday constant (96 485 C/mol)
h	Planck constant (Js)
J	Photocurrent density (mA cm^{-2})
J_{MAPD}	Maximum achievable photocurrent density (mA cm^{-2})
J_{sc}	Short-circuit current density (mA cm^{-2})
M_p	Fuel's molar mass (g/mol)
P_{out}	Output power (mW cm^{-2})
R_λ	Reflectance spectrum (%)
T_λ	Transmittance spectrum (%)
t_{dur}	Catalyst durability (h)
V	Voltage (V)
V_{oc}	Open-circuit voltage (V)
FE	Faradaic efficiency (%)
FF	Fill factor (%)

silicon (Si), have been investigated for PEC CO_2R systems and found to produce the reduction potential (E_{red}) required for CO_2R [28–32].

The photoanode, photocathode, and gas diffusion layer (GDL) are fundamental components of the electrocatalysis process [33,34]. The photoanode produces O_2 gas by oxidizing H_2O during the oxygen evolution reaction (OER), and the photocathode drives CO_2RR, eventually producing H_2 and hydrocarbon (C_2–C_3) fuels, such as carbon monoxide (CO), formic acid (HCOOH), methanol (CH_3OH), methane (CH_4), ethylene (C_2H_4), ethanol (C_2H_5OH), and propanol (C_3H_7O) [35,36]. The reduction of CO_2 occurs on the surface of cathodic metal catalysts deposited on GDL. GDL is a macroporous conductive carbon paper, supporting the mass transport of CO_2 and an increased J [37,38]. Several electrocatalysts of noble and functionalized transition metals are commonly used for OER, and noble and non-noble metal catalysts are used for CO_2RR to enhance reaction kinetic rates and Faradaic efficiency (FE) [39–41]. Liu et at. designed an amorphous Si-based photoanode for the CO_2R process and demonstrated that silver (Ag) and copper (Cu) exhibited FE of 90% and 53% for CO and C_2–C_3 fuel production, respectively [34]. Another photoanode used a-Si/TiO_2/Au heterostructures for CO_2R in PEC and exhibited excellent FE of 50%–90% and 50% for H_2 and CO fuel production, respectively [42]. Recently, some atomically dispersed Cu, nickel (Ni), palladium (Pd), zinc (Zn), iron (Fe), antimony (Sb), bismuth (Bi), and tin (Sn) catalysts have appeared as new catalysts for the CO_2R process, offering excellent FE and durability [43–48].

The photocatalytic CO_2R faces several critical challenges. Developing a commercially viable renewable fuel production technology requires a high J, selectivity, and stable operation with longevity [40]. Renewable fuel production can reach commercial viability with an efficient light-harvesting structure, fast charge carrier separation, and efficient charge transport to a catalytic active surface [49,50]. However, state-of-the-art (SOA) CO_2R techniques to produce renewable fuels suffer from poor selectivity of the end products, as the reaction pathway depends on several factors, including temperature, pressure,

the pH level of electrolyte, space charge polarization, and slow reaction kinetics [40,51].

The CO_2RR also suffers from large overpotential, product accumulation around the catalyst surface, and resistive losses in the cell, limiting the rate of CO_2RR and conversion into desired fuels [50,52]. The catalysts often degrade and lose catalytic activity during CO_2RR, seriously affecting the stable operation and durability [53,54]. Also, the corrosion and oxidation of the catalyst's surfaces drastically reduce the catalytic activity for CO_2R. With the availability of earth-abundant and low-cost fuels, there is little incentive to adopt new, large-scale energy technologies that pose considerable upfront technical and economic challenges [40,49]. The renewable fuels produced from a PEC CO_2R system must be cheap to become alternatives to commercial fossil fuels. Recently, some efforts at the techno-economic feasibility of CO_2 electroreduction processes have been reported considering proton exchange membrane, alkaline, and solid oxide electrolyzer systems [55–57]. However, a comprehensive and realistic investigation of PEC CO_2R systems toward commercial viability is still lacking, considering essential systems, materials, and operating costs.

In this work, to achieve commercial viability for the produced renewable fuels, we propose a PEC CO_2R system, where a crystalline Si (c-Si)-based triangle nano-strip structure as a photoanode efficiently absorbs solar energy. The cathode comprises a GDL, a two-dimensional conductive graphene sheet (2D-G), and metal catalysts. The optical properties, such as absorption spectrum, $A(\lambda)$, reflectance spectrum, $R(\lambda)$, and light intensity distribution for the proposed photoanode, have been calculated using the finite-difference time-domain (FDTD) method. The electrical simulations have been carried out using the three-dimensional (3D) finite element method (FEM) to determine the operating J, voltage (V), fill factor (FF), output power (P_{out}), and power-conversion efficiency (η_{PCE}). The obtained J and V for a unit cell of the proposed photoanode's structure are 35.65 mA cm^{-2} and 0.56 V, respectively, and the corresponding η_{PCE} is 20.01%.

We perform a comprehensive techno-economic analysis (TEA) of the proposed PEC CO_2R system, which converts solar energy into renewable fuels. In order to assess the techno-economic viability (TEV) of the produced renewable fuels, a general gross margin (GM) model has been developed considering the costs related to the photoabsorber, electrolyzer, catalyst, housing, fuel separation, carbon capture, bank interest, labor, and replacements. The effects of J, catalyst durability (t_{dur}), and catalyst cost (C_{cat}) are extensively investigated using the developed GM model to assess which produced renewable fuels are commercially viable. We further analyze the sensitivity of the renewable fuels' commercial viability considering the variations of the device performances and uncertainty in the critical cost parameters. To compare the production costs of different fuels, levelized fuel costs (LFCs) have been calculated using the gasoline gallon equivalent (gge) method. Based on the TEA, renewable H_2, C_3H_7OH, CO, and HCOOH fuels produced from the direct solar energy conversion using the proposed PEC CO_2R system are commercially competitive or better than their market prices. Such a TEA provides a valuable perspective on developing a sustainable PEC CO_2R system that helps the direct solar conversion of CO_2 into renewable fuels with better efficiency than SOA techniques.

2. Proposed photoelectrochemical carbon dioxide reduction

Fig. 1 schematically illustrates the proposed PEC CO_2R system at a conceptual level. The proposed PEC CO_2R system aims to ensure the TEV of the produced renewable fuels through innovative designs and using low-cost and earth-abundant materials, increasing the solar-to-fuel conversion efficiency and stability much more than SOA techniques. The proposed PEC system utilizes Si, transition metals and their oxides, polymers, and glass materials for CO_2R . Si is one of the most abundant elements on earth. Matured and relatively inexpensive technology can be used to fabricate Si-based devices [58,59]. Transition metals and their oxides are also being used in large-scale commercial devices due to their abundance and less costly manufacturing processes than novel materials [60].

The proposed photoanode consists of photo-absorbing semiconductor layers S_1 and S_2. S_1 is a triangle nano-strip structure, offering significant light absorption within the triangle cavities [61]. S_2 enhances light absorption at longer wavelengths and produces J by exciting electron–hole pairs. S_2 also reduces charge carrier recombination and enhances charge carrier transportation to the catalytic surfaces due to the shorter transportation length of charge carriers compared to the diffusion length within the thin-film substrate [62,63]. c-Si used for S_1 and S_2 in the proposed structure is a low-cost and commercially available earth-abundant material [59].

An ultra-thin protection layer (P_1) used between S_2 and metal foam (M_1) protects the degradation of S_2 and remarkably reduces surface state recombination [34]. TiO_2 and Ni are used for P_1 and M_1, respectively. The optimized P_1 thickness (t_p) of ~50 nm enhances stability by preventing semiconductor material degradation [34,64]. M_1 increases the mechanical strength of the photoanode with lightweight and thermal conductivity. The proposed structure has an M_1 of 5 mm thickness [65]. An effective photoanode catalyst (C_1) will be embedded into M_1 to enhance catalytic activity toward producing O_2 gas. Notably, the P_1–M_1–C_1 heterostructure contributes to efficient charge carrier separation and prevents recombination due to the produced space charge polarization and built-in electric field within the depletion layer [66].

A PEC CO_2R system must produce renewable fuels efficiently and selectively to make them commercially viable [61]. Desired catalytic performances can be achieved using a macroporous carbon matrix via polytetrafluoroethylene (PTFE) coating of GDL, a high conductive 2D material (M_2) deposited on GDL, and an effective metal catalyst (C_2) [20]. GDL is crucial in helping electron transport for CO_2RR and CO_2 distribution to the catalytic surface to produce renewable fuels [67]. Furthermore, GDL is a low-cost material with excellent catalytic performances suitable for large-scale commercialization. A 2D-G layer is used as M_2 to boost the electron transfer from GDL to the catalytic surface. C_2 is a layer of nanostructures or nanoholes, as shown in the bottom view in Fig. 1, coated with functionalized nanocomposite particles. Therefore, C_2 increases the catalytic active surface area and kinetic rate of CO_2RR. The maximum conversion of CO_2 and the selectivity of the produced fuel will be achieved using an effective catalyst—nanocomposite particles or a hybrid metal catalyst—and precise control of the operating parameters [39,41]. The catalyst's durability will be enhanced by suppressing the product accumulation on catalysts and controlling the cell parameters, such as pH, temperature, pressure, and electrolyte purity [33,68].

The left side of Fig. 1 shows the inlet of the electrolyte and CO_2 gas. The PTFE flow channel will drive them into the corresponding compartments and control the flow rates. Similarly, the outlet will exude O_2 gas into the air. The mixture of renewable products will proceed through the separation process, isolating individual renewable fuels. A complete stack container for the PEC CO_2R system will consist of different types of glasses, polymer materials, and aluminum plates, which are low-cost and commercially available [69,70].

3. Computational methodology

In this section, we present optical and electrical simulation models, including their related parameters. These models are used to determine the optimized parameters of the proposed photoanode structure and calculate the PEC CO_2R system's optical and electrical performances. This section also presents the techno-economic model and assumptions employed for a comprehensive analysis of the renewable fuels produced from CO_2R.

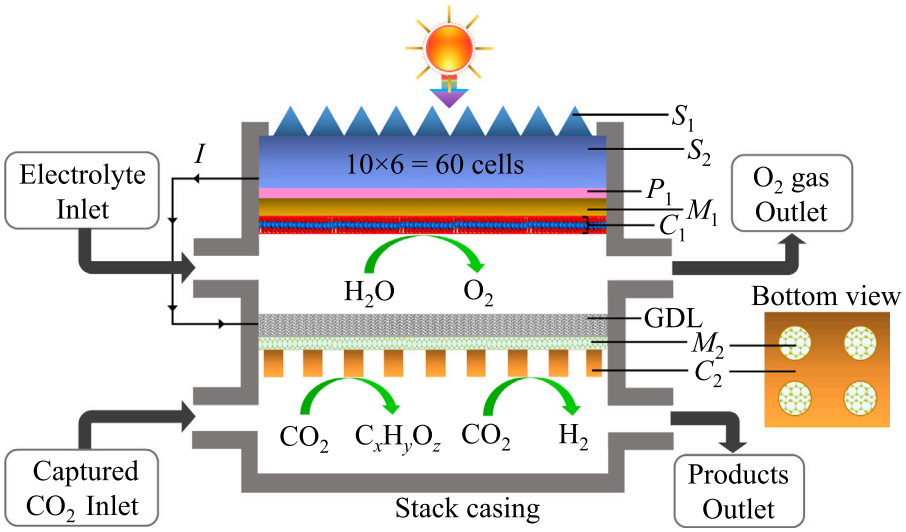

Fig. 1. Schematic illustration of a stack design for the proposed PEC CO_2R system.

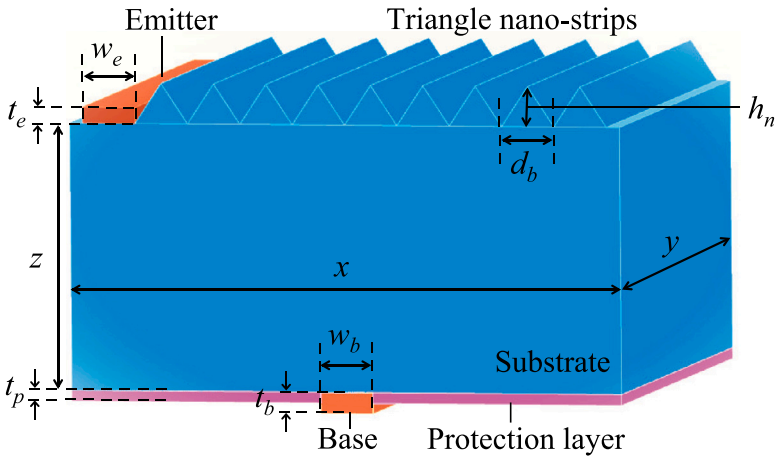

Fig. 2. Schematic illustration of the proposed photoanode structure with structural parameters for optical and electrical simulations.

3.1. Optical and electrical simulation models

We perform optical simulations using the 3D FDTD method for the proposed PEC system's photoanode structure, as illustrated in Fig. 2 [71]. The structure is periodic in the x- and y-directions, while a perfectly matched layer (PML) boundary is considered in the z-direction. We use a transverse electric (TE)-polarized Gaussian light pulse as the source, considering wavelengths from 300 to 1200 nm. Ag is used for the emitter, and aluminum (Al) is used for the base contact, offering good electrical conductivity, low resistance, and ohmic contact with semiconductors [72]. Table 1 shows the optimized parameters of the proposed structure obtained through optical simulations. We investigate the optical light intensity confined within the proposed structure and calculate $A(\lambda)$, $R(\lambda)$, and the solar absorbance efficiency (SAE). $A(\lambda)$ is determined from the transmittance spectrum, $T(\lambda)$, and $R(\lambda)$ as

$$A(\lambda) = 1 - T(\lambda) - R(\lambda). \tag{1}$$

SAE is calculated by the ratio between the absorbed and incident solar power as given by

$$\mathrm{SAE} = \frac{\int (\lambda/hc) A(\lambda) \Phi_{\mathrm{AM1.5G}}(\lambda)\, d\lambda}{\int (\lambda/hc) \Phi_{\mathrm{AM1.5G}}(\lambda)\, d\lambda}, \tag{2}$$

where $\Phi_{\mathrm{AM1.5G}}(\lambda)$ is the AM1.5 global solar irradiance [73], h is the Planck constant, and c is the speed of light.

We perform electrical simulations and calculate η_{PCE}, J vs. V, and P vs. V characteristics, where P is the converted electrical power. The electrical performances have been determined by solving the Gummel poon model using the 3D FEM [74,75]. However, J and V calculated in an ideal scenario are overestimated compared to non-ideal but realistic cases as inherent losses associated with electronic circuits and photoabsorbing materials are not considered in ideal cases [75,76]. The non-ideal effects, such as resistive losses, the Shockley–Read–Hall (SRH) effect, high-level injection of minority charge carriers, auger recombination, and radiative recombination losses, if considered, may make significant differences in the short-circuit current density (J_{sc}) and open-circuit voltage (V_{oc}) [77,78]. Therefore, we consider the non-ideal effects in this work based on the parameters given in Table S1. We also consider p-type doping for the photoanode semiconductor.

3.2. Gross margin model for techno-economic analysis

We have conducted a GM model-based TEA to determine the TEV of the produced renewable fuels from the PEC CO_2R system. The GM model evaluates the overall profitability of manufacturing activities by considering the relevant direct costs, including maintenance and operating costs [79]. It also considers critical cost factors and overheads to determine whether acceptable profit is produced from sales and hence assists in making strategic pricing decisions [80,81]. In practice, this model offers various advantages in the manufacturing process, such

Table 1
Optimized structural parameters of the proposed photoanode.

Parameter	Symbol	Optimized value	Parameter	Symbol	Optimized value
Thin-film length	x	20 μm	Thin-film width	y	20 μm
Thin-film height	z	5 μm	Triangle nano-strip base	d_b	1 μm
Triangle nano-strip height	h_n	0.75 μm	P_1 thickness	t_p	50 nm
Emitter thickness	t_e	200 nm	Base thickness	t_b	200 nm

as better control over the cost of goods sold (λ_{COGS}), improved cost management monitoring, identification of opportunities for growing profits from specific products, and the ability to analyze and justify strategic investment decisions [80].

In a previous study, Verma et al. developed a GM model for the electroreduction of CO_2 assuming polymer electrolyte membrane (PEM) electrolyzer system, excluding operation (λ_{op}) and labor (λ_{lab}) cost parameters [82]. The model by Verma et al. helps us benchmark the developed TEA model of this work. In this work, the GM model considers all the relevant cost parameters, such as costs related to photoanode (λ_{ph}), catalyst (λ_{cat}), electrolyte (λ_{elec}), stack casing (λ_{sc}), CO_2 capture (λ_{cp}), fuel separation (λ_{sep}), λ_{op}, and λ_{lab}, across practical scenarios. The model also considers the balance of plant (BOP) cost (λ_{BOP}), including the installation, contingency, site preparation, designing, and maintenance costs. The total λ_{BOP} is 40.2% (see Table S2) of the capital cost (λ_{cap}), meeting the DOE Forecourt analysis requirement [83]. This analysis also considers the bank interest imposed on the total expenses. The GM (expressed in %) is defined as the ratio between the profit and the revenue (λ_R), where the profit is calculated by subtracting the λ_{COGS} from the λ_R. Therefore, GM is written as [82,84]

$$GM = \frac{\lambda_R - \lambda_{COGS}}{\lambda_R}. \tag{3}$$

The required GM for a particular fuel may vary depending on the market demand and supply. However, GM > 0 is an essential condition for TEV, and usually GM $\gtrsim$ 30% is expected for a more realistic commercial viability [80,85].

The total λ_{COGS} in Eq. (3) is obtained by summing up λ_{cap}, λ_{cp}, λ_{sep}, λ_{BOP}, λ_{op}, and λ_{lab}. The PEC system development cost, λ_{cap}, comprises λ_{ph}, λ_{cat}, GDL cost (λ_{GDL}), λ_{elec}, λ_{sc}, and other necessary costs (λ_{nec}), consisting of PTFE flow channel, housing, and assembly costs. The λ_{ph}, λ_{cat}, λ_{GDL}, λ_{elec}, λ_{sc}, and λ_{nec} can be given by

$$\lambda_{ph} = C_{ph} t, \tag{4a}$$

$$\lambda_{cat} = \frac{C_{cat} W_{cat} A t}{t_{dur}}, \tag{4b}$$

$$\lambda_{GDL} = \frac{C_{GDL} A t}{t_{dur}}, \tag{4c}$$

$$\lambda_{elec} = C_{elec} Q t, \tag{4d}$$

$$\lambda_{sc} = C_{sc} t, \tag{4e}$$

$$\lambda_{nec} = C_{nec} t, \tag{4f}$$

where C_{ph} is the hourly installment payment of photoanode for each stack ($/h), C_{cat} is the catalyst cost ($/mg), W_{cat} is the catalyst loading (mg/cm^2), A is the electrode active surface area (cm^2), t_{dur} is the catalyst durability (h), C_{GDL} is the GDL cost per unit area ($/cm^2), C_{elec} is the cost of electrolyte per unit volume ($/mL), Q is the electrolyte purge flow rate (ml/h), C_{sc} is the hourly installment payment of stack-casing for each stack ($/h), C_{nec} is the hourly installment payment of other necessary costs for each stack ($/h), and t is the total running time (h) of the PEC CO_2R system.

Direct CO_2 capture technologies from the air source are more suitable for decarbonization, cost-effectiveness, and the ability to be installed in existing industrial sites [86,87]. We estimated λ_{cp} based on the cost analysis of these methods. λ_{cp} is expressed as $\lambda_{cp} = C_{cp} M_{CO_2} t$, where C_{cp} and M_{CO_2} are the CO_2 capture cost per unit mass ($/kg) and CO_2 mass captured per hour (kg/h), respectively.

The produced renewable fuels contain a mixture of gaseous and liquid fuels and the unreacted CO_2. It is essential to separate individual fuel from the mixture. It is also beneficial to reuse the unreacted CO_2. λ_{sep} can be estimated using the Sherwood plot [88,89]. In accordance with the plot, the separation cost of a particular fuel is inversely related to the weight fraction (w_p) of the separated fuel in the mixture so that $\lambda_{sep} \propto k_p/w_p$, where k_p is the separation cost of the separated fuel per unit mass ($/kg$_{mix}$). Thus, the overall λ_{sep} can be calculated incorporating the Faraday electrolysis law for the renewable fuels' production rates and is given by [82]

$$\lambda_{sep} = 36 \times 10^{-6} \times \frac{JAt}{F} \sum_p FE_p \frac{k_p M_p}{z_p w_p}, \tag{5}$$

where M_p is the produced fuel's molar mass (g/mol), F = 96 485 C/mol is the Faraday constant, z_p is the required number of electrons for CO_2R to produce the fuel, and FE_p is the produced fuel's Faradaic efficiency (%).

In this TEA, we assumed $\lambda_{op} = 0.025\lambda_{cap}$ and $\lambda_{lab} = 0.1\lambda_{cap}$ according to the U.S. Bureau of Labor Statistics (BLS) [90,91]. The λ_R in Eq. (3) for the produced renewable fuels from the PEC CO_2R system is calculated by incorporating the fuel production rate, estimated by Faraday electrolysis law, and the sales price of the fuel (C_p). Thus, λ_R is given by [82]

$$\lambda_R = 36 \times 10^{-6} \frac{JAt}{F} \sum_p FE_p \frac{C_p M_p}{z_p}. \tag{6}$$

Finally, the per-unit cost of a particular fuel ($/kg or $/gge) is estimated by dividing λ_{COGS} by the amount of produced fuel or gasoline gallon equivalent (gge) mass in terms of the combustion energy content.

3.3. Photoelectrochemical cell stack operation and techno-economic assumptions

To perform the TEA for the produced renewable fuels, it is essential to clarify several key factors related to the proposed system. These factors include the cell and stack parameters, λ_{cap}, and operating conditions. The cell and stack parameters are crucial for designing the PEC CO_2R system. λ_{cap} is associated with the materials required to develop the system. Furthermore, the costs associated with capturing CO_2 and separating individual renewable fuels from the mixtures are crucial when operating the system.

3.3.1. Photoelectrochemical cell stack operation

The PEC CO_2R system requires a minimum standard reduction potential (E^0_{cell}) to produce each renewable fuel, which varies depending on the produced fuel [93]. Table 2 shows the cathodic reaction processes for CO_2R into renewable fuels and the corresponding z_p and E^0_{cell}. Table 2 also shows the produced fuels' C_p and M_p. However, in practice, E_{red} must be $\gtrsim$1.6 V for CO_2R due to associated losses [94]. In this work, we designed a PEC stack with sixty unit cells of the proposed photoanode structure to provide sufficient applied V and operating J for converting CO_2 into renewable fuels with commercial viability. The electrical connection among the unit cells is categorized based on the output V and J of a unit cell described in Section 4.2.1. In this TEA, the dimension of each unit cell is 20 cm × 20 cm, providing an active surface area of 400 cm^2. The total number of the PEC stack (n_{stack}) is 100. The replacement cycle (t_{rmc}) is four years for the major components, such as the photoabsorbing structure, metal foam, and

Table 2
Standard reduction potential (E^0_{cell}) and cathodic reaction for CO_2R into renewable fuels [19,56,82,92].

Fuel	C_p ($/kg)	M_p (g/mol)	Cathodic reaction process	z_p	E^0_{cell} (V)
H_2	4.5	2.016	$2H^+ + 2e^- \rightarrow H_2$	2	1.23
CO	0.60	28.01	$CO_2 + 2H^+ + 2e^- \rightarrow CO + H_2O$	2	1.34
CH_4	0.18	16.04	$CO_2 + 8H^+ + 8e^- \rightarrow CH_4 + 2H_2O$	8	1.06
C_2H_4	1.30	28.05	$2CO_2 + 12H^+ + 12e^- \rightarrow C_2H_4 + 4H_2O$	12	1.17
HCOOH	0.74	46.02	$CO_2 + 2H^+ + 2e^- \rightarrow HCOOH$	2	1.48
CH_3OH	0.50	32.04	$CO_2 + 6H^+ + 6e^- \rightarrow CH_3OH + H_2O$	6	1.21
C_2H_5OH	1.00	46.07	$2CO_2 + 12H^+ + 12e^- \rightarrow C_2H_5OH + 3H_2O$	12	1.15
C_3H_7OH	1.43	60.094	$3CO_2 + 18H^+ + 18e^- \rightarrow C_3H_7OH + 5H_2O$	18	1.135

Table 3
Operating parameters for the proposed PEC CO_2R system.

Parameters	Symbol	Nominal value
Active area per unit cell	A_{cell}	400 cm^2
Number of unit cell per stack	n_{cell}	60 units
Total number of PEC stack	n_{stack}	100 units
Total active area of the system	A	240 m^2
System running time per year	t_{year}	4000 h
Replacement discount factor	r_d	12%
Replacement cycle	t_{rmc}	4 years
Bank interest rate	r	5%
Loan term	t_{lt}	20 years

stack casing, including a 12% discount factor (r_d) of λ_{cap} [95]. We used a 5% bank interest rate (r) and a loan term (t_{lt}) of 20 years. The running time (t_{year}) of the PEC CO_2R system is 4000 h per year. Table 3 lists the PEC CO_2R system operation parameters.

3.3.2. Capital cost

The photoabsorbing material c-Si is low-cost and suitable for large-scale industrial manufacturing [96]. We estimated the design and fabrication cost of the proposed structure from related efforts available in the literature. The estimated manufacturing cost for a single stack is 0.48 $/W, including material, wafer, design, and metalization costs [97–99]. The total converted electrical power is 48 kW based on the electrical simulation for the PEC CO_2R system. C_{ph} is estimated at 10.4×10^{-2} $/h, comprising the photoabsorber, protection layer, and Ni metal foam cost. The photoanode catalysts used in this analysis are nickel oxide (NiO_x), iridium dioxide (IrO_2), platinum (Pt), and manganese dioxide (MnO_2), and the photocathode catalysts are Cu, Ag, Sn, Zn, gold (Au), and lead (Pb). The loading rate of the photoanode catalyst (W_{cat}) is 5.0 mg/cm^2. The GDL is assumed to be 2 mm thick. The photocathode catalyst loading may vary from 0.12 to 0.25 mg/cm^2 depending on the catalysts (see Table S3). The t_{dur} of the catalysts and the GDL is assumed to be 4000 h for the base case [82]. The 2.0 M potassium hydroxide (KOH) electrolyte solution has a purge flow rate of 60 ml min^{-1}, evaluated by the base-case production rate for each stack. The detailed costs of the catalysts, GDL, and electrolyte are given in Table S3.

The closed stack casing will be implemented using different types of glasses, polymer materials, and aluminum plates, considering the advanced design in terms of commercial specifications. Based on the sufficient volume for the reduction process within the stack and outside protection, we estimated $C_{sc} = 19.68 \times 10^{-2}$ $/h in this analysis. The other necessary elements of the PTFE flow channel, housing, and assembly costs are assumed to be 300 $/year, 6 $/month, and 8 $ for each stack, respectively [100]. Therefore, λ_{nec} is estimated as 73.60×10^{-2} $/h in this TEA.

3.3.3. Carbon dioxide capture and fuel separation costs

Monoethanolamine (MEA) and solid direct air capture (S-DAC) techniques are often used to capture CO_2 from flue gases and the air [87,101]. The MEA technique uses amine-based solvents that capture CO_2 through adsorption and desorption processes from flue gases. The extracted CO_2 cost in the MEA technique is 70.0 $/ton [101]. On the other hand, the S-DAC technique captures carbon from the air using solid sorbent filters that bind with CO_2. The estimated cost of CO_2 capture using this technique is 100–600 $/ton [102]. However, the S-DAC technique extracts CO_2 from its low-contraction air and is suitable for large-scale production with sustainability. Therefore, we considered the S-DAC techniques for this TEA. We calculated the M_{CO_2} considering the maximum production rate of CO_2R and the auxiliary amount of CO_2, immobile into the stack and tube of the storage tank. Based on the previous literature on TEA, we assumed FE = 75% as the base case for the proposed PEC CO_2R system [83,103].

In the reduction processes of CO_2, the produced fuels can be liquid, such as HCOOH, CH_3OH, C_2H_5OH, and C_3H_7OH, and gaseous, such as H_2, CH_4, and C_2H_4. We calculated $k_p = 0.001$ and 0.006 $/$kg_{mix}$ for gaseous and liquid fuels, respectively, from the Sherwood plots to estimate the cost of fuel separation [104].

4. Results and discussion

This section presents the results of optical, electrical, and techno-economic analyses. The optical and electrical performances demonstrate the efficiency of solar energy absorption and conversion into electricity. Furthermore, the results of the techno-economic analysis, based on the GM model, offer details on the commercial viability of the renewable fuels produced from CO_2R under various conditions.

4.1. Optical and electrical performances

The photoanode of the PEC CO_2R system must absorb the incident solar energy efficiently to convert it into electrical energy. We vary the structural parameters of the proposed structure to determine the optimized values, as given in Table 1. Fig. 3(a) shows $A(\lambda)$ and $R(\lambda)$ for the optimized proposed structure, and 96.23% light absorption is obtained considering wavelengths from 300 to 1200 nm. The light absorption efficiency reaches ~100% at $\lambda \sim 600$ nm due to the strong resonances created in the photoabsorbing material. Also, the proposed structure enhances light absorption at longer wavelengths due to the strong spatial confinement of light within the triangle nano-strips and the thin-film substrate. Thus, $A(\lambda)$ is >60% for longer wavelengths, outperforming a planar c-Si structure [105]. Fig. 3(b) shows light intensity through electric field distribution in the proposed photoanode structure with two triangle nano-strips at $\lambda = 700$ nm. The maximum obtained SAE is 91.81% considering 300–1200 nm wavelengths. For the optimized proposed structure, the maximum achievable photocurrent density (J_{MAPD}) is 41.77 mA cm^{-2} determined by

$$J_{MAPD} = \int \frac{q\lambda}{hc} A(\lambda)\phi_{AM1.5G}(\lambda)\, d\lambda, \tag{7}$$

where q is the elementary electronic charge. The calculated J_{MAPD} does not include the surface and bulk recombinations, i.e., each absorbed photon creates an electron–hole pair.

In practice, it is necessary to assess the recombination and resistive losses through an electrical simulation model. Fig. 4(a) and (b) show the J–V and P–V characteristics for a unit cell of the proposed photoanode structure, respectively, where the obtained operating J, V, and P_{out} are 35.65 mA cm^{-2}, 0.56 V, and 20.01 mWcm^{-2}, respectively.

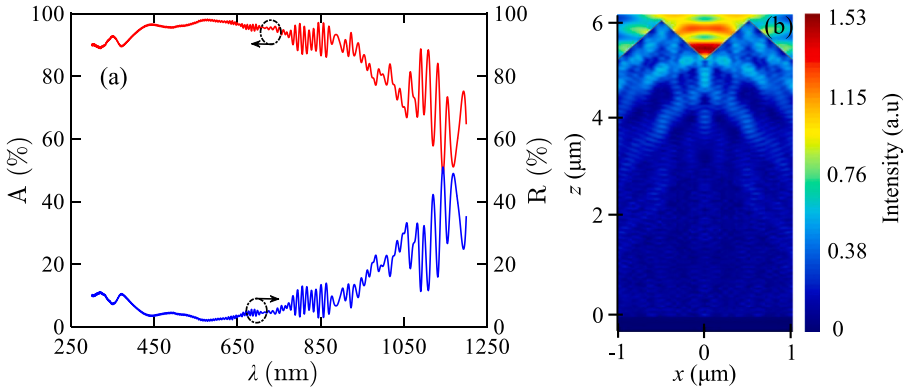

Fig. 3. (a) Absorbance, $A(\lambda)$, and reflectance spectra, $R(\lambda)$, of the proposed photoanode structure. (b) Light intensity distribution on the xz cross-sectional plane for the proposed photoanode structure at $\lambda = 700$ nm.

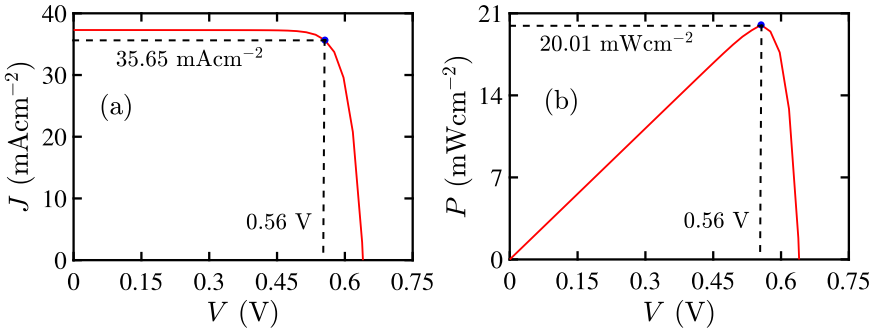

Fig. 4. (a) J vs. V and (b) P vs. V characteristics of a unit cell of the proposed photoanode of the CO_2R system.

However, the short circuit current density (J_{sc}) is 37.30 mA cm^{-2}, which is lower than J_{MAPD} due to the losses. The obtained FF at the operating condition is 83.8%. In our TEA, we considered $J_{cell} = 35$ mA cm^{-2}, $V_{cell} = 0.55$ V, and $P_{out} = 19.25$ mWcm^{-2}, where J_{cell}, V_{cell}, and P_{cell} are the unit cell operating current density, potential, and output power, respectively, for the proposed PEC CO_2R system.

4.2. Techno-economic analysis

To investigate the TEV of the produced renewable fuels, it is necessary to assess the GM profit, which depends on various critical parameters of the proposed PEC CO_2R system. These parameters include J, t_{dur}, C_{cat}, and FE. The preference of optimal values for these parameters is crucial for making commercially viable renewable fuels from CO_2R. Additionally, it is necessary to conduct a comprehensive sensitivity analysis under different conditions to understand how these parameters can affect the production cost of a specific fuel, and hence, the commercial viability.

4.2.1. Gross margin vs. current density

The operating J represents the rate of CO_2RR, and it will vary with the different possibilities of the series-parallel connections of the designed stack's sixty unit cells. Besides, it is necessary to provide sufficient E_{red} for the CO_2R process from electrical connections. In practice, E_{red} varies from 1.60 to 3.5 V depending on the associated losses and electrochemical performances of the PEC CO_2R system [83,106]. Therefore, we consider three connections among the sixty unit cells in a stack: (i) The base-case scenario with fifteen branches connected in parallel with each branch consisting of four series-connected cells, producing $J_b = 525$ mA cm^{-2} and $V_b = 2.2$ V, (ii) the worst-case scenario with ten branches connected in parallel with each branch consisting of six series-connected cells, producing $J_w = 350$ mA cm^{-2} and $V_w = 3.3$ V, and (iii) the optimistic-case scenario with twenty branches connected in parallel with each branch consisting of three series-connected cells, producing $J_o = 700$ mA cm^{-2} and $V_o = 1.65$ V. Thus, the operating J varies from 350 to 700 mA cm^{-2}. The condition for TEV that GM > 0 critically depends on the minimum value of J required to produce fuels [82].

During commercial production, λ_{op} and λ_{lab} impact an industry's profitability and should be considered in a TEA [90,91]. By accurately estimating and controlling λ_{op} and λ_{lab}, an industry can maintain competitive market pricing, ultimately driving higher profitability. This TEA investigates GM of the produced fuels with and without λ_{op} and λ_{lab}. Fig. 5(a) and (b) show GM vs. J without and with considering λ_{op} and λ_{lab}, respectively. In both cases, HCOOH, CO, H_2, and C_3H_7OH fuels have GM > 0 within the operating window. Without considering λ_{op} and λ_{lab}, HCOOH and CO fuels have GM > 50% at $J = 700$ mA cm^{-2} and GM > 0 even at $J = 350$ mA cm^{-2}. However, with λ_{op} and λ_{lab}, the GM of CO fuel reaches below 50% at $J = 700$ mA cm^{-2} and GM < 0 at $J = 350$ mA cm^{-2}. For HCOOH, the GM does not vary noticeably with or without considering λ_{op} and λ_{lab}. The other two fuels, H_2 and C_3H_7OH, have GM > 10% near the end of the operating window without considering λ_{op} and λ_{lab}. However, by including these costs, the GM for H_2 and C_3H_7OH fuels decreases to 5%, considered a critical condition for sustainable commercialization [85]. Other fuels do not show a positive GM within the operating window. However, C_2H_5OH, C_2H_4, and CH_3OH fuels will have a positive GM if the operating J can be increased to 1000 mA cm^{-2} using more unit cells in a stack and efficient new photoabsorbing structure whose development and manufacturing cost must fulfill the commercial viability.

4.2.2. Effects of catalyst durability

A catalyst's durability and catalysis ability affect the TEV and the production rate of a PEC CO_2R system significantly. In this TEA, we considered that the catalyst has t_{dur} of 4000 h in the base case while 6000 h in the optimistic case [82,107]. Thus, the maximum operating

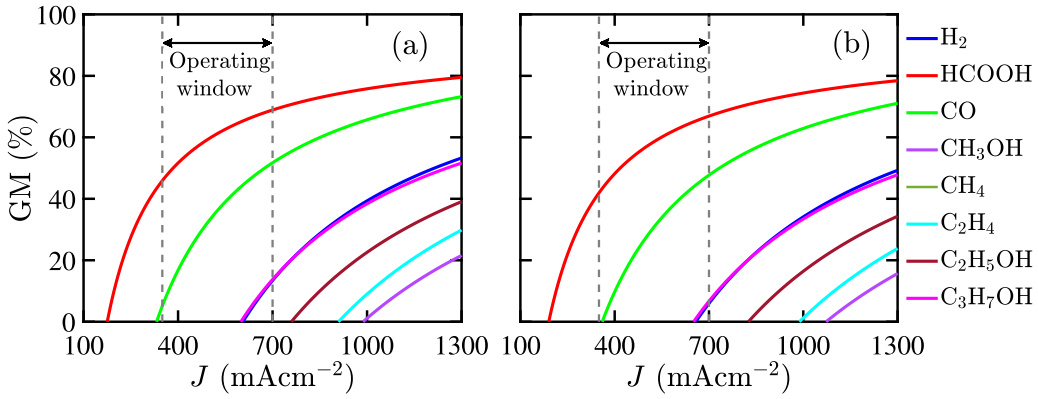

Fig. 5. Gross margin (GM) against current density (J) for CO_2R into renewable fuels (a) without λ_{op} and λ_{lab}, and (b) with λ_{op} and λ_{lab}.

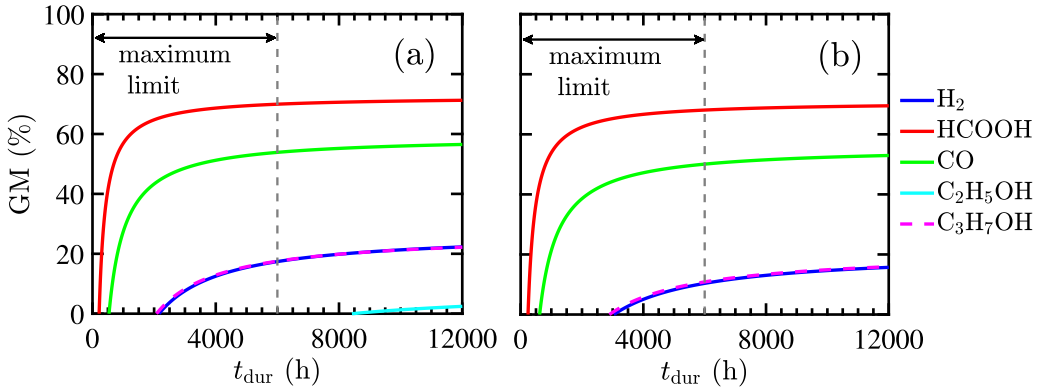

Fig. 6. Gross margin (GM) against catalyst durable (t_{dur}) for CO_2R into renewable fuels (a) without λ_{op} and λ_{lab}, and (b) with λ_{op} and λ_{lab}. In each case, $J = 700$ mA cm^{-2}.

period of the catalyst is t_{dur} = 0–6000 h. The effect of t_{dur} on GM of the produced fuels is presented in Fig. 6(a) and (b) without and with considering λ_{op} and λ_{lab}, respectively, where J = 700 mA cm^{-2}. For HCOOH and CO fuels, GM > 20% when t_{dur} > 1000 h, and GM > 40% when t_{dur} > 2000 h for both without and with λ_{op} and λ_{lab}. For H_2 and C_3H_7OH fuels, the GM becomes positive at t_{dur} = 2000 h when λ_{op} and λ_{lab} are not considered, and it is ~20% at t_{dur} = 6000 h. With λ_{op} and λ_{lab}, the GM becomes positive at t_{dur} = 3000 h, and it is ~10% at t_{dur} = 6000 h. Therefore, the produced HCOOH, CO, H_2, and C_3H_7OH fuels are commercially viable for t_{dur} = 3000–6000 h.

4.2.3. Effects of catalyst cost variation and faradaic efficiency

The cost and FE of catalysts used on the PEC CO_2R system are crucial in determining the TEV of the produced renewable fuels [24,36]. An expensive catalyst with an excellent FE or a cheaper catalyst with a poor FE might both be economically feasible at times. The typically used catalysts for OER, such as NiO_x, IrO_2, MnO_2, and Pt, exhibit an excellent FE of $\gtrsim$90% and a low overpotential loss [108–111]. Different metal and transitional metal catalysts are used for the CO_2R process based on their FE to produce the desired renewable fuels efficiently [112,113]. Fe, Ni, Pt, and titanium (Ti) metal electrocatalysts favor producing H_2 fuel efficiently. In contrast, Ag, Au, and Zn metals are primarily selective to CO [114]. Ti, Bi, Pb, Sn, mercury (Hg), cadmium (Cd), and indium (In) materials produce HCOOH during the CO_2R process [115]. Notably, Cu is the only material that helps produce C_2–C_3 fuels, such as C_2H_4, C_2H_5OH, and C_3H_7O [82,116].

Generally, the FE of metal catalysts varies from 50 to 98% depending on the catalytic activity and the produced fuel from the CO_2R process [68,117]. Fig. 7 shows the effects of anodic and cathodic catalyst costs on the GM of the produced fuels when the anodic (cathodic) FE is 50%, 75%, and 98%, and the cathodic (anodic) FE is kept at 90%. The effect of anodic catalyst cost ($C_{cat,an}$) varying from 10^{-6} to 10^{0} \$/mg on the GM of the produced fuels is illustrated in Fig. 7(a)–(c). HCOOH and CO fuels are commercially viable in all three cases. The maximum cost of $C_{cat,an}$ for HCOOH and CO fuels is estimated to be 10^{-1} and $10^{-1.4}$ \$/mg, respectively, for GM $\geq$ 0 at FE = 98%. In contrast, H_2 and C_3H_7OH fuels are commercially viable at FE of 75% and 98% only. The maximum cost of $C_{cat,an}$ for H_2 and C_3H_7OH with GM $\geq$ 0 is $10^{-2.95}$ \$/mg at FE = 75%, and 10^{-2} \$/mg at FE = 98%. C_2H_5OH fuel has a positive GM at FE = 98% only with $C_{cat,an} < 10^{-2.6}$ \$/mg.

Fig. 7(d)–(f) show the impact of cathodic catalyst cost ($C_{cat,ca}$) on the GM of the produced fuels. For HCOOH and CO fuels, the maximum $C_{cat,ca}$ should be $\lesssim 10^{0.1}$ \$/mg at FE = 50% for GM > 0. $C_{cat,ca}$ may increase if FE increases. The catalysts reported in this analysis, such as Ag, Au, Zn, Sb, and Pb, can produce commercially viable HCOOH and CO fuels. On the other hand, H_2 and C_3H_7OH fuels exhibit commercial viability at FE = 75 and 98%. The maximum $C_{cat,ca}$ is $10^{-1.2}$ \$/mg at FE = 75% that is much higher than the catalyst costs of Pt, Ag, Au, and Cu, i.e., these catalysts are commercially feasible for the production of H_2 and C_3H_7OH fuels. At FE = 98%, a little room of the positive GM for C_2H_5OH fuel might be promising within the broad ranges of the catalyst cost that support the use of Cu and other catalysts. However, it is difficult for the Cu catalyst to show such a high FE in the PEC CO_2R system. Therefore, a new catalytic material, which will exhibit high FE and low cost for commercially viable C_2H_5OH production, still needs to be explored. Furthermore, we calculated the efficiency of photocatalytic CO_2R for CO, HCOOH, H_2, and C_3H_7OH fuels. The results are presented in Table 4, including a comparison with those in the existing literature.

4.2.4. Sensitivity analysis of the desired products

Based on the above TEA, the produced HCOOH, CO, H_2, and C_3H_7OH fuels from the PEC CO_2R system show great promise for

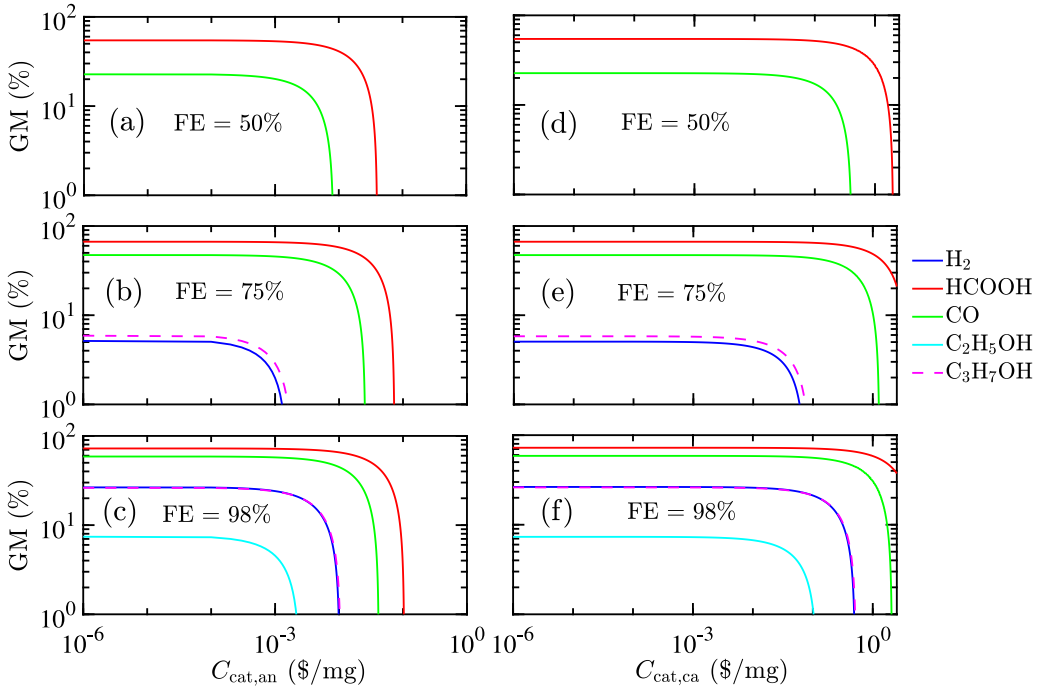

Fig. 7. Gross margin (GM) against anodic catalyst cost ($C_{cat,an}$) for FE (a) 50%, (b) 75%, and (c) 98%, and against cathodic catalyst cost ($C_{cat,ca}$) for FE (d) 50%, (e) 75%, and (f) 98%. In each case, $J = 700$ mA cm^{-2} and λ_{op} and λ_{lab} are considered.

Table 4
Comparison of the efficiency of photocatalytic CO_2R for CO, HCOOH, H_2, and C_3H_7OH fuels with those in the existing literature.

Fuel	Catalyst	FE (%)	Production (mmol g^{-1} h^{-1})	Ref.	Fuel	Catalyst	FE (%)	Production (mmol g^{-1} h^{-1})	Ref.
CO	Co-MOL@GO	95	18.02	[118]	HCOOH	ZnV_2O_6	48.78	2.89	[119]
	Co-Co_2P@NPC	79.1	~ 70	[120]		RGO/ZnV_2O_6	25.96	1.94	[119]
	GDL/2D-G/Ag	90	56.82	This work		GDL/2D-G/Pb	40	25.23	This work
H_2	Pt/T	> 80	16.1	[121]	C_3H_7OH	Rh_1Co_3/MCM-41	~ 18	1.77	[122]
	Pt/Cu(0.1)/T	> 90	23.7	[121]		Rh-Co/rGO	61.70	~ 3.5	[123]
	GDL/2D-G/Pt	80	48.96	This work		GDL/2D-G/Cu	40	2.81	This work

Table 5
Multiplication factors of the sensitive cost parameters for sensitivity analysis.

Description of parameters	Worst case	Base case	Optimistic case
Multiplication factor of J (m_J)	0.67	1	1.33
Multiplication factor of FE (m_{FE})	0.67	1	1.31
Multiplication factor of λ_{BOP} (m_{BOP})	1.37	1	0.63
Multiplication factor of λ_{cap} (m_{cap})	1.25	1	0.75
Multiplication factor of λ_{cp} (m_{cp})	1.25	1	0.75
Multiplication factor of λ_{elec} (m_{elec})	1.25	1	0.75

large-scale commercialization. λ_{COGS} included different parameters that might critically affect the production cost of a particular fuel. To investigate the production cost of these fuels, we performed a sensitivity analysis considering the base-, worst-, and optimistic-case scenarios of several key cost parameters. We assume FE = 50 and 98% for the worst- and optimistic-case scenarios, respectively [117]. λ_{BOP} increases and decreases by 15% for the worst- and optimistic-case scenarios, respectively. For the other parameters, such as λ_{cap}, λ_{cp}, and λ_{elec}, we consider an increase and decrease by 25% from the base-case scenario for the worst- and optimistic-case scenarios, respectively. Table 5 shows the related cost parameters' multiplication factors for the worst- and optimistic-case scenarios concerning the base-case scenario.

Fig. 8 shows the sensitivity analysis results for the produced fuels, where the dashed black and red lines indicate the fuel production cost in the base-case scenario and the commercial price, respectively. The blue bars on the right and the green bars on the left of the base-case line represent the fuel production cost in the worst- and optimistic-case scenarios, respectively. In this sensitivity analysis, we vary a particular cost parameter considering the worst- and optimistic-case scenarios while keeping other parameters at the base case.

In this analysis, the base case production cost of H_2 fuel is 5.65 $/kg, while the commercial price is 4.50 $/kg. In the optimistic case, the enhanced J and FE decrease the H_2 fuel production cost below the market price level, but the worst case increases the production cost by 2.73 $/kg. The optimistic- and worst-case scenarios of λ_{BOP}, λ_{cap}, and λ_{elec} affect the decrease and increase of the fuel production cost equally. The optimistic case of λ_{cap} offers the fuel production cost below the commercial price range. On the other hand, there is a negligible effect on the fuel production cost for the λ_{cp} variation. For C_3H_7OH fuel, the base case production cost is 1.80 $/kg, while the commercial price is 1.43 $/kg. The effect of sensitivity analysis for C_3H_7OH fuel is almost similar to the H_2 fuel. Remarkably, the optimistic values of J, FE, and λ_{cap} individually contribute to decreasing the production cost of H_2 and C_3H_7OH fuels within the commercial price range. Fig. 8(c)–(d) show the sensitivity analysis of CO and HCOOH fuels. The commercial prices of CO and HCOOH fuels are 0.60 $/kg and 0.74 $/kg, respectively. The base case production cost for both is lower than the commercial price, and the worst case of the individual cost parameter also keeps the production cost within the market price level. Therefore, CO and HCOOH fuels are promising for feasible commercialization, considering the sensitivity of the cost parameters.

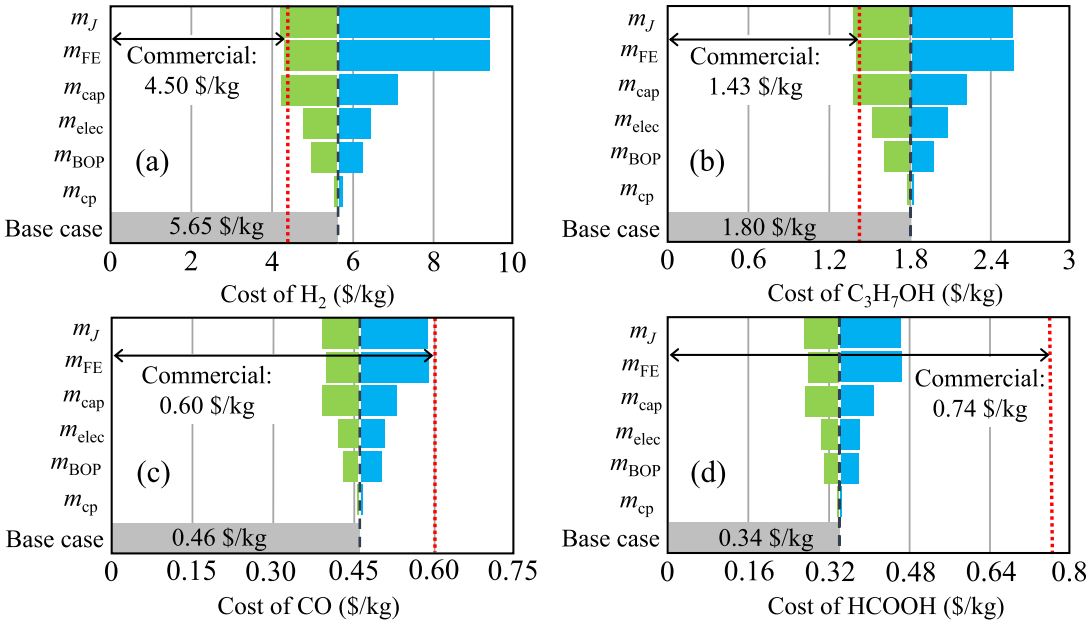

Fig. 8. Sensitivity analysis under the optimistic- (green bars) and worst-case (blue bars) scenarios for CO_2R into (a) H_2, (b) C_3H_7OH, (c) CO, and (d) HCOOH fuels. The red and black dashed lines indicate the commercial price and base case fuel production cost obtained from the TEA.

5. Levelized cost of the desired products

The preceding TEA for the proposed PEC CO_2R system helps to comprehend the TEV of the produced H_2, C_3H_7OH, CO, and HCOOH fuels. Among the fuels, H_2 and CO are gaseous fuels, while H_2 is more demanding for the upcoming sustainable energy development due to higher gravimetric and volumetric energy density than other fuels [124,125] . In addition, H_2 meets zero carbon emissions without adverse environmental impact during utilization, as the byproducts are only heat and water. Based on the present scenario, the dynamic demand of global H_2 is estimated from 73 to 158 Mt by 2030, 300 Mt by 2040, and 568 Mt by 2050 [126]. On the contrary, CO contains carbon, which may affect greenhouse gases and global warming. However, the CO and H_2 mixture as syngas ($CO+H_2$) is combustive and can be used as a fuel for internal combustion engines in cars to replace gasoline. It can also be used in industrial metal fabrication and the Fischer–Tropsch process to produce hydrocarbons, such as diesel, methane, methanol, and dimethyl ether (DME) [83]. Both HCOOH and C_3H_7OH fuels are in the liquid phase. HCOOH is used in direct formic acid fuel cells (DFAFCs), portable electronic devices, and electric vehicles. C_3H_7OH is used in fuel cells and the pharmaceutical industry as a solvent, e.g., resins, cellulose esters, and disinfecting agents.

Several sensitive cost parameters may deviate the fuel production cost from the base case, changing the value illustrated in the sensitivity analysis. The variations of J, FE, and λ_{cap} critically affect the fuel production cost more significantly than other cost parameters. Assuming all cost parameters vary simultaneously, the estimated LFCs of the produced fuels are summarized in Fig. 9. To produce economically viable fuels in the proposed PEC CO_2R system, CO and HCOOH fuels show lower LFCs under the base- and optimistic-case scenarios than commercial prices. However, the LFCs under the worst case are 15.94 $/gge and 23.21 $/gge for CO and HCOOH fuels, respectively, much higher than commercial price levels. Notably, if any two parameters out of J, FE, and λ_{cap} under the worst case recede to the optimistic case, the LFCs will be estimated at 4.28 $/gge and 7.95 $/gge for CO and HCOOH fuels, respectively, offering commercial viability. The projected LFCs under the optimistic case are 2.32 $/gge and 19.35 $/gge for H_2 and C_3H_7OH, respectively, which are much lower than commercial prices, showing significant economic viability. However, the production cost of H_2 and C_3H_7OH fuels is much higher than the commercial price under the base- and worst-case scenarios. Remarkably, if any one parameter out of J, FE, and λ_{cap} under the base case recedes to the optimistic case, the LFCs will decrease to the commercial price levels for both. Therefore, in the proposed PEC CO_2R system, aiming to produce H_2, C_3H_7OH, CO, and HCOOH fuels can make more sense than other carbon-based fuels.

In terms of equivalent energy cost through gge, H_2 is a more cost-effective fuel compared to C_3H_7OH, CO, and HCOOH fuels considering commercial prices, where the cost of H_2, C_3H_7OH, CO, and HCOOH fuels are 4.80 $/gge, 37.36 $/gge, 5.63 $/gge, and 17.63 $/gge, respectively. Under the base case, CO is more cost-effective than other fuels. The LFCs of CO, HCOOH, H_2, and C_3H_7OH fuels under the base case are 4.32 $/gge, 8.10 $/gge, 6.03 $/gge, and 47.04 $/gge, respectively. Thus, CO, HCOOH, and H_2 fuels can be comparatively more techno-economic viable based on the equivalent energy cost compared to other fuels.

6. Summary and outlook

In summary, we presented an innovative design for a PEC that efficiently converts solar energy into renewable fuels using the CO_2R process. The photoanode structure of the PEC CO_2R system used a triangle nano-strip structure and thin-film substrate, achieving light absorption efficiency of >90% and η_{PCE} of >20%. We developed a generalized GM model that considered the critical cost parameters to assess the TEV of the renewable fuels produced from the PEC CO_2R system. We also analyzed the TEV against essential device factors, such as J, t_{dur}, FE, and C_{cat}. For H_2, C_3H_7OH, CO, and HCOOH — the renewable fuels with more promising TEV — we investigated LFCs and sensitivity against the uncertainty of the key cost parameters considering the worst-, base-, and optimistic-case scenarios. CO and HCOOH fuels show significant promises of being commercially viable in the base-case scenario for the proposed PEC CO_2R system. In addition, H_2, C_3H_7OH fuel production costs are within the commercial price range. The TEA of the proposed PEC CO_2R system shows excellent promises for renewable fuels from CO_2R toward large-scale industrialization that can benefit both decarbonization and the economy.

This work provides valuable perspectives on developing sustainable green energy technology considering key cost parameters. Such analyses can also be beneficial for other relevant technologies to assess

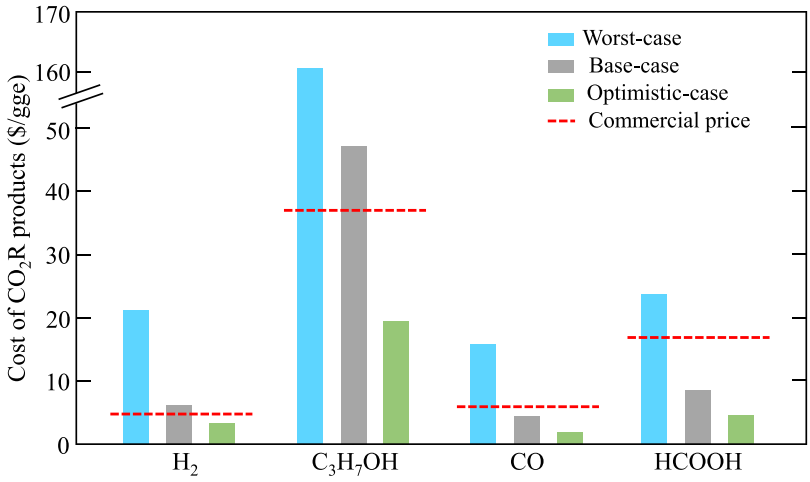

Fig. 9. Levelized fuel costs (LFCs) of H_2, C_3H_7OH, CO, and HCOOH fuels from CO_2R under the worst-, base-, and optimistic-case scenarios.

commercial viability. A comprehensive TEA considering crucial system parameters can enhance the large-scale production of CO_2R fuels and their adoption in markets. It is essential to achieve pure chemical fuels with efficient photocatalytic CO_2R to minimize production costs for competitive markets. Therefore, there is a need to focus on developing efficient and cost-effective electrocatalysts or photocatalysts with enhanced FE and minimum overpotential losses. Overall, the PEC or electrochemical reduction of CO_2 and its comprehensive TEA could play a significant role in making a strategic energy solution policy that will immensely contribute to the future renewable energy infrastructure.

CRediT authorship contribution statement

Abdul Ahad Mamun: Writing – original draft, Validation, Methodology, Investigation, Formal analysis. **Muhammad Anisuzzaman Talukder:** Writing – review & editing, Supervision, Methodology, Conceptualization.

Declaration of competing interest

The authors declare that they have no known competing financial interests or personal relationships that could have appeared to influence the work reported in this paper.

Data availability

Data will be made available on request.

Appendix A. Supplementary data

Supplementary material related to this article can be found online at https://doi.org/10.1016/j.enconman.2024.119038.

References

[1] Rockström J, Gaffney O, Rogelj J, Meinshausen M, Nakicenovic N, Schellnhuber HJ. A roadmap for rapid decarbonization. Science 2017;355(6331):1269–71.
[2] Luderer G, Pehl M, Arvesen A, Gibon T, Bodirsky BL, De Boer HS, Fricko O, Hejazi M, Humpenöder F, Iyer G, et al. Environmental co-benefits and adverse side-effects of alternative power sector decarbonization strategies. Nature Commun 2019;10(1):5229.
[3] Masson-Delmotte V, Zhai P, Pörtner H-O, Roberts D, Skea J, Shukla PR, et al. Global warming of 1.5° C: IPCC special report on impacts of global warming of 1.5° C above pre-industrial levels in context of strengthening response to climate change, sustainable development, and efforts to eradicate poverty. Cambridge University Press; 2022.
[4] Yu T, Chen Y. Effects of elevated carbon dioxide on environmental microbes and its mechanisms: A review. Sci Total Environ 2019;655:865–79.
[5] Jacobson TA, Kler JS, Hernke MT, Braun RK, Meyer KC, Funk WE. Direct human health risks of increased atmospheric carbon dioxide. Nat Sustain 2019;2(8):691–701.
[6] Mardani A, Streimikiene D, Cavallaro F, Loganathan N, Khoshnoudi M. Carbon dioxide (CO_2) emissions and economic growth: A systematic review of two decades of research from 1995 to 2017. Sci Total Environ 2019;649:31–49.
[7] Rovere A, Ryan DD, Vacchi M, Dutton A, Simms AR, Murray-Wallace CV. The world atlas of last interglacial shorelines (version 1.0). Earth Syst Sci Data 2023;15(1):1–23.
[8] National Centers for Environmental Information (NCEI). NOAA National centers for environmental information, monthly global climate report for annual 2023. 2024, https://www.ncei.noaa.gov/access/monitoring/monthly-report/global/202313.
[9] Parry I, Black MS, Vernon N. Still not getting energy prices right: A global and country update of fossil fuel subsidies. International Monetary Fund; 2021.
[10] Osman AI, Chen L, Yang M, Msigwa G, Farghali M, Fawzy S, Rooney DW, Yap P-S. Cost, environmental impact, and resilience of renewable energy under a changing climate: a review. Environ Chem Lett 2023;21(2):741–64.
[11] Rennert K, Errickson F, Prest BC, Rennels L, Newell RG, Pizer W, Kingdon C, Wingenroth J, Cooke R, Parthum B, et al. Comprehensive evidence implies a higher social cost of CO_2. Nature 2022;610(7933):687–92.
[12] Habert G, Miller SA, John VM, Provis JL, Favier A, Horvath A, Scrivener KL. Environmental impacts and decarbonization strategies in the cement and concrete industries. Nat Rev Earth Environ 2020;1(11):559–73.
[13] Soergel B, Kriegler E, Weindl I, Rauner S, Dirnaichner A, Ruhe C, Hofmann M, Bauer N, Bertram C, Bodirsky BL, et al. A sustainable development pathway for climate action within the UN 2030 Agenda. Nature Clim Change 2021;11(8):656–64.
[14] Barber J, Tran PD. From natural to artificial photosynthesis. J R Soc Interface 2013;10(81):20120984.
[15] Krewald V, Retegan M, Pantazis DA. Principles of natural photosynthesis. Solar Energy Fuels 2016;23–48.
[16] Liu Z, Deng Z, Davis SJ, Giron C, Ciais P. Monitoring global carbon emissions in 2021. Nat Rev Earth Environ 2022;3(4):217–9.
[17] Nitopi S. Understanding the factors that govern activity and selectivity of the electrochemical carbon dioxide reduction reaction on copper catalysts. Stanford University; 2019.
[18] Hartley A, Turnock S. What are the benefits of reducing global CO_2 emissions to net-zero by 2050? Weather 2022;77(1):27–8.
[19] Nitopi S, Bertheussen E, Scott SB, Liu X, Engstfeld AK, Horch S, Seger B, Stephens IE, Chan K, Hahn C, et al. Progress and perspectives of electrochemical CO_2 reduction on copper in aqueous electrolyte. Chem Rev 2019;119(12):7610–72.
[20] Chen C, Kotyk JFK, Sheehan SW. Progress toward commercial application of electrochemical carbon dioxide reduction. Chem 2018;4(11):2571–86.
[21] Wang B, Lu X, Lundin S-TB, Kong H, Wang J, Su B, Wang H. Thermodynamic analysis and optimization of solar methane dry reforming enhanced by chemical hydrogen separation. Energy Convers Manage 2022;268:116050.
[22] Wang H, Liu T, Kong H. Solar CO_2 splitting coupling with PV, photon-enhanced thermionic emission cell and SOEC for efficient full-spectrum utilization in a wide temperature range. Appl Energy 2024;367:123360.
[23] Si F, Wei M, Li M, Xie X, Gao Q, Cai X, Zhang S, Peng F, Fang Y, Yang S. Natural light driven photovoltaic-electrolysis water splitting with 12.7% solar-to-hydrogen conversion efficiency using a two-electrode system grown with metal foam. J Power Sources 2022;538:231536.

[24] Lianos P. Review of recent trends in photoelectrocatalytic conversion of solar energy to electricity and hydrogen. Appl Catal B 2017;210:235–54.

[25] Kumaravel V, Bartlett J, Pillai SC. Photoelectrochemical conversion of carbon dioxide (CO_2) into fuels and value-added products. ACS Energy Lett 2020;5(2):486–519.

[26] Pang H, Masuda T, Ye J. Semiconductor-based photoelectrochemical conversion of carbon dioxide: Stepping towards artificial photosynthesis. Chem– Asian J 2018;13(2):127–42.

[27] Shan B, Vanka S, Li T-T, Troian-Gautier L, Brennaman MK, Mi Z, Meyer TJ. Binary molecular-semiconductor p–n junctions for photoelectrocatalytic CO_2 reduction. Nat Energy 2019;4(4):290–9.

[28] LaTempa TJ, Rani S, Bao N, Grimes CA. Generation of fuel from CO_2 saturated liquids using a p-Si nanowire n-TiO_2 nanotube array photoelectrochemical cell. Nanoscale 2012;4(7):2245–50.

[29] Kim JH, Magesh G, Kang HJ, Banu M, Kim JH, Lee J, Lee JS. Carbonate-coordinated cobalt co-catalyzed $BiVO_4/WO_3$ composite photoanode tailored for CO_2 reduction to fuels. Nano Energy 2015;15:153–63.

[30] Liu L-X, Fu J, Jiang L-P, Zhang J-R, Zhu W, Lin Y. Highly efficient photoelectrochemical reduction of CO_2 at low applied voltage using 3D Co-Pi/$BiVO_4/SnO_2$ nanosheet array photoanodes. ACS Appl Mater Interfaces 2019;11(29):26024–31.

[31] Zhou X, Liu R, Sun K, Chen Y, Verlage E, Francis SA, Lewis NS, Xiang C. Solar-driven reduction of 1 atm of CO_2 to formate at 10% energy-conversion efficiency by use of a TiO_2-protected III–V tandem photoanode in conjunction with a bipolar membrane and a Pd/C cathode. ACS Energy Lett 2016;1(4):764–70.

[32] Zhang Y, Luc W, Hutchings GS, Jiao F. Photoelectrochemical carbon dioxide reduction using a nanoporous Ag cathode. ACS Appl Mater Interfaces 2016;8(37):24652–8.

[33] Chen P, Zhang Y, Zhou Y, Dong F. Photoelectrocatalytic carbon dioxide reduction: fundamental, advances and challenges. Nano Mater Sci 2021;3(4):344–67.

[34] Liu B, Wang T, Wang S, Zhang G, Zhong D, Yuan T, Dong H, Wu B, Gong J. Back-illuminated photoelectrochemical flow cell for efficient CO_2 reduction. Nature Commun 2022;13(1):7111.

[35] Morikawa T, Sato S, Sekizawa K, Suzuki TM, Arai T. Solar-driven CO_2 reduction using a semiconductor/molecule hybrid photosystem: from photocatalysts to a monolithic artificial leaf. Acc Chem Res 2021;55(7):933–43.

[36] Ulmer U, Dingle T, Duchesne PN, Morris RH, Tavasoli A, Wood T, Ozin GA. Fundamentals and applications of photocatalytic CO_2 methanation. Nature Commun 2019;10(1):3169.

[37] Xing Z, Hu L, Ripatti DS, Hu X, Feng X. Enhancing carbon dioxide gas-diffusion electrolysis by creating a hydrophobic catalyst microenvironment. Nature Commun 2021;12(1):136.

[38] Yang K, Kas R, Smith WA, Burdyny T. Role of the carbon-based gas diffusion layer on flooding in a gas diffusion electrode cell for electrochemical CO_2 reduction. ACS Energy Lett 2020;6(1):33–40.

[39] Wang C, Guan S, Zhang H, Shen R, Yuan H, Li B. Perspectives on two-dimensional ultra-thin materials in energy catalysis and storage. APL Mater 2023;11(5).

[40] Birdja YY, Pérez-Gallent E, Figueiredo MC, Göttle AJ, Calle-Vallejo F, Koper MT. Advances and challenges in understanding the electrocatalytic conversion of carbon dioxide to fuels. Nat Energy 2019;4(9):732–45.

[41] Qiao J, Liu Y, Hong F, Zhang J. A review of catalysts for the electroreduction of carbon dioxide to produce low-carbon fuels. Chem Soc Rev 2014;43(2):631–75.

[42] Li C, Wang T, Liu B, Chen M, Li A, Zhang G, Du M, Wang H, Liu SF, Gong J. Photoelectrochemical CO_2 reduction to adjustable syngas on grain-boundary-mediated a-Si/TiO_2/Au photocathodes with low onset potentials. Energy Environ Sci 2019;12(3):923–8.

[43] Yang HB, Hung S-F, Liu S, Yuan K, Miao S, Zhang L, Huang X, Wang H-Y, Cai W, Chen R, et al. Atomically dispersed Ni (i) as the active site for electrochemical CO_2 reduction. Nat Energy 2018;3(2):140–7.

[44] Zhao K, Nie X, Wang H, Chen S, Quan X, Yu H, Choi W, Zhang G, Kim B, Chen JG. Selective electroreduction of CO_2 to acetone by single copper atoms anchored on N-doped porous carbon. Nature Commun 2020;11(1):2455.

[45] He Q, Lee JH, Liu D, Liu Y, Lin Z, Xie Z, Hwang S, Kattel S, Song L, Chen JG. Accelerating CO_2 electroreduction to CO over Pd single-atom catalyst. Adv Funct Mater 2020;30(17):2000407.

[46] Zhang E, Wang T, Yu K, Liu J, Chen W, Li A, Rong H, Lin R, Ji S, Zheng X, et al. Bismuth single atoms resulting from transformation of metal–organic frameworks and their use as electrocatalysts for CO_2 reduction. J Am Chem Soc 2019;141(42):16569–73.

[47] Jiang Z, Wang T, Pei J, Shang H, Zhou D, Li H, Dong J, Wang Y, Cao R, Zhuang Z, et al. Discovery of main group single Sb–N_4 active sites for CO_2 electroreduction to formate with high efficiency. Energy Environ Sci 2020;13(9):2856–63.

[48] Wang Y, Liu Y, Liu W, Wu J, Li Q, Feng Q, Chen Z, Xiong X, Wang D, Lei Y. Regulating the coordination structure of metal single atoms for efficient electrocatalytic CO_2 reduction. Energy Environ Sci 2020;13(12):4609–24.

[49] He J, Janaky C. Recent advances in solar-driven carbon dioxide conversion: expectations versus reality. ACS Energy Lett 2020;5(6):1996–2014.

[50] Lu Q, Rosen J, Zhou Y, Hutchings GS, Kimmel YC, Chen JG, Jiao F. A selective and efficient electrocatalyst for carbon dioxide reduction. Nature Commun 2014;5(1):3242.

[51] Mustafa A, Lougou BG, Shuai Y, Wang Z, Razzaq S, Zhao J, Tan H. Theoretical insights into the factors affecting the electrochemical reduction of CO_2. Sustain Energy Fuels 2020;4(9):4352–69.

[52] Lin J, Zhang Y, Xu P, Chen L. CO_2 Electrolysis: Advances and challenges in electrocatalyst engineering and reactor design. Mater Rep: Energy 2023;100194.

[53] Yang F, Elnabawy AO, Schimmenti R, Song P, Wang J, Peng Z, Yao S, Deng R, Song S, Lin Y, et al. Bismuthene for highly efficient carbon dioxide electroreduction reaction. Nature Commun 2020;11(1):1088.

[54] Navarro-Jaén S, Virginie M, Bonin J, Robert M, Wojcieszak R, Khodakov AY. Highlights and challenges in the selective reduction of carbon dioxide to methanol. Nat Rev Chem 2021;5(8):564–79.

[55] Shin H, Hansen KU, Jiao F. Techno-economic assessment of low-temperature carbon dioxide electrolysis. Nat Sustain 2021;4(10):911–9.

[56] Jouny M, Luc W, Jiao F. General techno-economic analysis of CO_2 electrolysis systems. Ind Eng Chem Res 2018;57(6):2165–77.

[57] Na J, Seo B, Kim J, Lee CW, Lee H, Hwang YJ, Min BK, Lee DK, Oh H-S, Lee U. General technoeconomic analysis for electrochemical coproduction coupling carbon dioxide reduction with organic oxidation. Nature Commun 2019;10(1):5193.

[58] Dabrowski J, et al. Silicon surfaces and formation of interfaces: Basic science in the industrial world. World Scientific; 2000.

[59] Liu F, Zeng Q, Li J, Hao X, Ho-Baillie A, Tang J, Green MA. Emerging inorganic compound thin film photovoltaic materials: Progress, challenges and strategies. Mater Today 2020;41:120–42.

[60] Ebhota WS, Jen T-C. Efficient low-cost materials for solar energy applications: roles of nanotechnology. In: Recent developments in photovoltaic materials and devices. IntechOpen; 2018.

[61] Chen H-Y, Lu H-L, Ren Q-H, Zhang Y, Yang X-F, Ding S-J, Zhang DW. Enhanced photovoltaic performance of inverted pyramid-based nanostructured black-silicon solar cells passivated by an atomic-layer-deposited Al_2O_3 layer. Nanoscale 2015;7(37):15142–8.

[62] Shah A, Torres P, Tscharner R, Wyrsch N, Keppner H. Photovoltaic technology: the case for thin-film solar cells. Science 1999;285(5428):692–8.

[63] Massiot I, Cattoni A, Collin S. Progress and prospects for ultrathin solar cells. Nat Energy 2020;5(12):959–72.

[64] Liu B, Wang S, Feng S, Li H, Yang L, Wang T, Gong J. Double-side Si photoelectrode enabled by chemical passivation for photoelectrochemical hydrogen and oxygen evolution reactions. Adv Funct Mater 2021;31(3):2007222.

[65] Song T-s, Fei K, Zhang H, Yuan H, Yang Y, Ouyang P, Xie J. High efficiency microbial electrosynthesis of acetate from carbon dioxide using a novel graphene–nickel foam as cathode. J Chem Technol Biotechnol 2018;93(2):457–66.

[66] Luo Z, Ye X, Zhang S, Xue S, Yang C, Hou Y, Xing W, Yu R, Sun J, Yu Z, et al. Unveiling the charge transfer dynamics steered by built-in electric fields in BiOBr photocatalysts. Nature Commun 2022;13(1):2230.

[67] Rabiee H, Ge L, Zhang X, Hu S, Li M, Yuan Z. Gas diffusion electrodes (GDEs) for electrochemical reduction of carbon dioxide, carbon monoxide, and dinitrogen to value-added products: a review. Energy Environ Sci 2021;14(4):1959–2008.

[68] Pei Y, Zhong H, Jin F. A brief review of electrocatalytic reduction of CO_2–Materials, reaction conditions, and devices. Energy Sci Eng 2021;9(7):1012–32.

[69] Dhanumalayan E, Joshi GM. Performance properties and applications of polytetrafluoroethylene (PTFE)—a review. Adv Compos Hybrid Mater 2018;1:247–68.

[70] Axinte E. Glasses as engineering materials: A review. Mater Des 2011;32(4):1717–32.

[71] Gedney S. Introduction to the finite-difference time-domain (FDTD) method for electromagnetics. Springer Nature; 2022.

[72] Nehate SD, Prakash A, Mani PD, Sundaram KB. Work function extraction of indium tin oxide films from MOSFET devices. ECS J Solid State Sci Technol 2018;7(3):P87.

[73] Center RRD. Reference solar spectral irradiance: ASTM G-173. vol. 21, Golden, CO: National Renewable Energy Laboratory; 2009, p. 2018, accessed July.

[74] Sischka F. GUMMEL-Poonbipolarmodel. vol. 86, Munich: Agilent Technologies; 1990.

[75] Lumerical Inc. Optoelectronic modeling. 2020, https://www.lumerical.com/learn/whitepapers/optoelectronic-modeling/.

[76] Khaled A, Hameed MFO, Rahman B, Grattan K, Obayya S, Hussein M. Characteristics of silicon nanowire solar cells with a crescent nanohole. Opt Express 2020;28(21):31020–33.

[77] Hosseini SR, Bahramgour M, Sefidi PY, Mashayekh AT, Moradi A, Delibas N, Hosseini MG, Niaei A. Investigating the effect of non-ideal conditions on the performance of a planar $CH_3NH_3PbI_3$-based perovskite solar cell through SCAPS-1D simulation. Heliyon 2022;8(11).

[78] Mamun AA, Karim J, Talukder MA. Design and analysis of an efficient crystalline silicon-based thin-film solar cell inspired by Chlamydomonas reinhardtii. Sol Energy 2024;279:112777.
[79] Nariswari TN, Nugraha NM. Profit growth: impact of net profit margin, gross profit margin and total assests turnover. Int J Finance Bank Stud (2147-4486) 2020;9(4):87–96.
[80] Evmenchik OS, Niyazbekova SU, Seidakhmetova FS, Mezentceva TM. The role of gross profit and margin contribution in decision making. In: Socio-economic systems: paradigms for the future. Springer; 2021, p. 1393–404.
[81] Andrianto A, Amin A. The effect of gross profit margin, intellectual capital, investment opportunity set on firm value with earnings management as an intervening variable. J Soc Res 2023;2(10):3428–50.
[82] Verma S, Kim B, Jhong H-RM, Ma S, Kenis PJ. A gross-margin model for defining technoeconomic benchmarks in the electroreduction of CO_2. ChemSusChem 2016;9(15):1972–9.
[83] Spurgeon JM, Kumar B. A comparative technoeconomic analysis of pathways for commercial electrochemical CO_2 reduction to liquid products. Energy Environ Sci 2018;11(6):1536–51.
[84] Farris PW, Bendle N, Pfeifer P, Reibstein D. Marketing metrics: The definitive guide to measuring marketing performance. Pearson Education; 2010.
[85] Kemmerer JE, Lu J. Profitability and royalty rates across industries: Some preliminary evidence. KPMG Global Valuation Institute; 2012, November.
[86] Qiu Y, Lamers P, Daioglou V, McQueen N, de Boer H-S, Harmsen M, Wilcox J, Bardow A, Suh S. Environmental trade-offs of direct air capture technologies in climate change mitigation toward 2100. Nature Commun 2022;13(1):3635.
[87] Erans M, Sanz-Pérez ES, Hanak DP, Clulow Z, Reiner DM, Mutch GA. Direct air capture: process technology, techno-economic and socio-political challenges. Energy Environ Sci 2022;15(4):1360–405.
[88] Sherwood TK. Mass transfer between phases, vol. 33, Pennsylvania State University; 1959.
[89] King CJ, Council NR, et al. Separation & purification: Critical needs and opportunities. National Academies; 1987.
[90] Mayfield E, Jenkins J. Influence of high road labor policies and practices on renewable energy costs, decarbonization pathways, and labor outcomes. Environ Res Lett 2021;16(12):124012.
[91] Klemeš J, Bulatov I, Cockerill T. Techno-economic modelling and cost functions of CO_2 capture processes. Comput Chem Eng 2007;31(5–6):445–55.
[92] US Department of Energy. Alternative fuels data center. https://afdc.energy.gov/fuels/prices.html.
[93] Wu J, Huang Y, Ye W, Li Y. CO_2 Reduction: from the electrochemical to photochemical approach. Adv Sci 2017;4(11):1700194.
[94] Chen Y, Li CW, Kanan MW. Aqueous CO_2 reduction at very low overpotential on oxide-derived Au nanoparticles. J Am Chem Soc 2012;134(49):19969–72.
[95] Shaner MR, Atwater HA, Lewis NS, McFarland EW. A comparative technoeconomic analysis of renewable hydrogen production using solar energy. Energy Environ Sci 2016;9(7):2354–71.
[96] Dang H. Nanostructured semiconductor device design in solar cells. 2015.
[97] Liu Z, Sofia SE, Laine HS, Woodhouse M, Wieghold S, Peters IM, Buonassisi T. Revisiting thin silicon for photovoltaics: a technoeconomic perspective. Energy Environ Sci 2020;13(1):12–23.
[98] Louwen A, Van Sark W, Schropp R, Faaij A. A cost roadmap for silicon heterojunction solar cells. Sol Energy Mater Sol Cells 2016;147:295–314.
[99] Chang NL, Zheng J, Wu Y, Shen H, Qi F, Catchpole K, Ho-Baillie A, Egan RJ. A bottom-up cost analysis of silicon–perovskite tandem photovoltaics. Prog Photovolt, Res Appl 2021;29(3):401–13.
[100] Alibaba. High pressure separate electromagnetism for measuring conductive liquids water measurement acid flow meter. https://www.alibaba.com/showroom/ptfe-flow-meter.html.
[101] Raksajati A, Ho MT, Wiley DE. Reducing the cost of CO_2 capture from flue gases using aqueous chemical absorption. Ind Eng Chem Res 2013;52(47):16887–901.
[102] Service RF. Cost plunges for capturing carbon dioxide from the air. https://www.science.org/content/article/cost-plunges-capturing-carbon-dioxide-air.
[103] Agarwal AS, Rode E, Sridhar N, Hill D. Conversion of CO_2 to value added chemicals: Opportunities and challenges. In: Handbook of climate change mitigation and adaptation. Springer; 2022, p. 1585–623.
[104] Dahmus JB, Gutowski TG. What gets recycled: an information theory based model for product recycling. Environ Sci Technol 2007;41(21):7543–50.
[105] Peters M, Rüdiger M, Bläsi B, Platzer W. Electro–optical simulation of diffraction in solar cells. Opt Express 2010;18(104):A584–93.
[106] Küngas R. Electrochemical CO_2 reduction for CO production: comparison of low-and high-temperature electrolysis technologies. J Electrochem Soc 2020;167(4):044508.
[107] Yu H, Danilovic N, Wang Y, Willis W, Poozhikunnath A, Bonville L, Capuano C, Ayers K, Maric R. Nano-size IrO_x catalyst of high activity and stability in PEM water electrolyzer with ultra-low iridium loading. Appl Catal B 2018;239:133–46.
[108] Elmacı G, Ertürk AS, Sevim M, Metin Ö. MnO_2 Nanowires anchored on mesoporous graphitic carbon nitride (MnO_2@ mpg-C_3N_4) as a highly efficient electrocatalyst for the oxygen evolution reaction. Int J Hydrog Energy 2019;44(33):17995–8006.
[109] Kumar M, Meena B, Subramanyam P, Suryakala D, Subrahmanyam C. Recent trends in photoelectrochemical water splitting: The role of cocatalysts. NPG Asia Mater 2022;14(1):88.
[110] Reier T, Oezaslan M, Strasser P. Electrocatalytic oxygen evolution reaction (OER) on Ru, Ir, and Pt catalysts: a comparative study of nanoparticles and bulk materials. ACS Catal 2012;2(8):1765–72.
[111] Huang L, Wei M, Qi R, Dong C-L, Dang D, Yang C-C, Xia C, Chen C, Zaman S, Li F-M, et al. An integrated platinum-nanocarbon electrocatalyst for efficient oxygen reduction. Nature Commun 2022;13(1):6703.
[112] Franco F, Rettenmaier C, Jeon HS, Cuenya BR. Transition metal-based catalysts for the electrochemical CO_2 reduction: from atoms and molecules to nanostructured materials. Chem Soc Rev 2020;49(19):6884–946.
[113] Liu X, Xiao J, Peng H, Hong X, Chan K, Nørskov JK. Understanding trends in electrochemical carbon dioxide reduction rates. Nature Commun 2017;8(1):15438.
[114] Vayenas CG, White RE, Gamboa-Aldeco ME. Modern aspects of electrochemistry 42, vol. 42, Springer Science & Business Media; 2008.
[115] Hussain J, Jónsson H, Skúlason E. Calculations of product selectivity in electrochemical CO_2 reduction. ACS Catal 2018;8(6):5240–9.
[116] Schouten KJP, Qin Z, Pérez Gallent E, Koper MT. Two pathways for the formation of ethylene in CO reduction on single-crystal copper electrodes. J Am Chem Soc 2012;134(24):9864–7.
[117] Monteiro MC, Philips MF, Schouten KJP, Koper MT. Efficiency and selectivity of CO_2 reduction to CO on gold gas diffusion electrodes in acidic media. Nature Commun 2021;12(1):4943.
[118] Wang J-W, Qiao L-Z, Nie H-D, Huang H-H, Li Y, Yao S, Liu M, Zhang Z-M, Kang Z-H, Lu T-B. Facile electron delivery from graphene template to ultrathin metal-organic layers for boosting CO_2 photoreduction. Nature Commun 2021;12(1):813.
[119] Bafaqeer A, Tahir M, Amin NAS. Synergistic effects of 2D/2D ZnV_2O_6/RGO nanosheets heterojunction for stable and high performance photo-induced CO_2 reduction to solar fuels. Chem Eng J 2018;334:2142–53.
[120] Xu Y, Mo J, Fu Z-C, Liu S, Yang Z, Fu W-F. An exceptionally efficient Co-Co_2P@N, P-codoped carbon hybrid catalyst for visible light-driven CO_2-to-CO conversion. Chem Eur J 2018;24(34):8596–602.
[121] Grigioni I, Dozzi MV, Bernareggi M, Chiarello GL, Selli E. Photocatalytic CO_2 reduction vs. H_2 production: The effects of surface carbon-containing impurities on the performance of TiO_2-based photocatalysts. Catal Today 2017;281:214–20.
[122] Biswas AN, Xie Z, Xia R, Overa S, Jiao F, Chen JG. Tandem electrocatalytic–thermocatalytic reaction scheme for CO_2 conversion to C_3 oxygenates. ACS Energy Lett 2022;7(9):2904–10.
[123] Chang J, Yao Y, Liu X. Bimetallic Rh-Co nanoparticles supported on reduced graphene oxide for ethylene hydroformylation: Influence of feed gas proportion. In: AIP conference proceedings. vol. 2924, AIP Publishing; 2024.
[124] van Renssen S. The hydrogen solution? Nature Clim Change 2020;10(9):799–801.
[125] Fareza AR, Nugroho FAA, Abdi FF, Fauzia V. Nanoscale metal oxides–2D materials heterostructures for photoelectrochemical water splitting—a review. J Mater Chem A 2022;10(16):8656–86.
[126] Mamun AA, Billah A, Talukder MA. Enhancing hydrogen evolution reaction using iridium atomic monolayer on conventional electrodes: A first-principles study. Int J Hydrog Energy 2024;59:982–90.